Monthly Notices
of the
ROYAL ASTRONOMICAL SOCIETY

MNRAS **453,** L83–L87 (2015) doi:10.1093/mnrasl/slv110

ALMA and *Herschel* reveal that X-ray-selected AGN and main-sequence galaxies have different star formation rate distributions

J. R. Mullaney,[1⋆] D. M. Alexander,[2] J. Aird,[3] E. Bernhard,[1] E. Daddi,[4] A. Del Moro,[2] M. Dickinson,[5] D. Elbaz,[4] C. M. Harrison,[2] S. Juneau,[4] D. Liu,[4] M. Pannella,[6] D. Rosario,[7] P. Santini,[8] M. Sargent,[9] C. Schreiber,[4] J. Simpson[2] and F. Stanley[2]

[1]*Department of Physics and Astronomy, The University of Sheffield, Hounsfield Road, Sheffield S3 7RH, UK*
[2]*Centre of Extragalactic Astronomy, Department of Physics, Durham University, South Road, Durham DH1 3LE, UK*
[3]*Institute of Astronomy, University of Cambridge, Madingley Road, Cambridge CB3 0HA, UK*
[4]*Laboratoire AIM, CEA/DSM-CNRS-Université Paris Diderot, Irfu/Service d'Astrophysique, CEA-Saclay, Orme des Merisiers, F-91191 Gif-sur-Yvette, France*
[5]*National Optical Astronomy Observatories, 950 N Cherry Avenue, Tucson, AZ 85719, USA*
[6]*Universitäts-Sternwarte München, Scheinerstr. 1, D-81679 München, Germany*
[7]*Max-Planck-Institut für Extraterrestrische Physik (MPE), Postfach 1312, D-85741 Garching, Germany*
[8]*INAF–Osservatorio Astronomico di Roma, via di Frascati 33, I-00040 Monte Porzio Catone, Roma, Italy*
[9]*Astronomy Centre, Department of Physics and Astronomy, University of Sussex, Brighton BN1 9QH, UK*

Accepted 2015 July 29. Received 2015 July 21; in original form 2015 June 17

ABSTRACT

Using deep *Herschel* and ALMA observations, we investigate the star formation rate (SFR) distributions of X-ray-selected active galactic nucleus (AGN) host galaxies at $0.5 < z < 1.5$ and $1.5 < z < 4$, comparing them to that of normal, star-forming (i.e. 'main-sequence', or MS) galaxies. We find that 34–55 per cent of AGNs in our sample have SFRs at least a factor of 2 below that of the average MS galaxy, compared to ≈15 per cent of all MS galaxies, suggesting significantly different SFR distributions. Indeed, when both are modelled as lognormal distributions, the mass and redshift-normalized SFR distributions of X-ray AGNs are roughly twice as broad, and peak ≈0.4 dex lower, than that of MS galaxies. However, like MS galaxies, the normalized SFR distribution of AGNs in our sample appears not to evolve with redshift. Despite X-ray AGNs and MS galaxies having different SFR distributions, the linear-mean SFR of AGNs derived from our distributions is remarkably consistent with that of MS galaxies, and thus with previous results derived from stacked *Herschel* data. This apparent contradiction is due to the linear-mean SFR being biased by bright outliers, and thus does not necessarily represent a true characterization of the typical SFR of X-ray AGNs.

Key words: galaxies: active – galaxies: evolution – galaxies: statistics.

1 INTRODUCTION

Today's most successful models of galaxy evolution predict that the energy released via accretion on to supermassive black holes (hereafter BHs) has played an important role in dictating how today's galaxies have grown and evolved (e.g. Schaye et al. 2015). As such, understanding the connection between galaxy growth via star formation and the growth of their resident BHs is one of the key challenges facing current extragalactic research (see Alexander & Hickox 2012, for a review). There are now numerous lines of empirical evidence in support of time-averaged/integrated BH growth correlating with star formation in their host galaxies; for example, (a) the tight proportionality between BH mass and galaxy bulge mass (e.g. Gebhardt et al. 2000); (b) the similar cosmic histories of the volume-averaged BH growth and star formation rates (hereafter SFR; e.g. Silverman et al. 2008; Aird et al. 2015); and, more directly, (c) the correlation between average BH growth and SFR among the star-forming galaxy population (e.g. Mullaney et al. 2012b; Chen et al. 2013; Delvecchio et al. 2015; Rodighiero et al. 2015). However, it is still far from clear what physical processes (e.g. feedback processes/common fuel supply/common triggering mechanism) connect BH growth to star formation to produce these average trends.

One of the primary means of making progress in this area has been to measure the SFRs and specific SFRs (i.e. SFR per unit stellar mass, or sSFR) of galaxies hosting growing BHs (witnessed as active galactic nuclei, or AGNs) and search for correlations or

⋆E-mail: j.mullaney@sheffield.ac.uk

differences (versus the non-AGN population) that may signify a causal connection. The *Herschel Space Observatory* (hereafter *Herschel*) has played a major role in progressing this science by providing an obscuration-independent view of star formation that is largely uncontaminated by emission from the AGN. However, with even the deepest *Herschel* surveys detecting $\lesssim$50 per cent of the AGN population, most studies have resorted to averaging (often via stacking analysis, but see Stanley et al. 2015) to characterize the (s)SFRs of the AGN population. These studies have typically reported that the average SFRs of AGNs trace that of star-forming 'main-sequence' (hereafter MS) galaxies (e.g. Harrison et al. 2012; Mullaney et al. 2012a; Santini et al. 2012; Rosario et al. 2013; Stanley et al. 2015), i.e. the dominant population of star-forming galaxies whose SFRs are roughly proportional to their stellar mass (i.e. sSFR $\approx$ constant), with a constant of proportionality that increases with redshift (e.g. Daddi et al. 2007; Noeske et al. 2007). However, as averages can be biased by bright outliers, it is feasible that these findings are being driven upwards by a few bright sources (e.g. fig. 14 of Rosario et al. 2015). Here, we test this by combining deep *Herschel* and ALMA observations to instead constrain the *distribution* of host galaxy SFRs of a sample of X-ray-selected AGNs and comparing it to that of MS galaxies. We adopt $H_0 = 71\,\mathrm{km\,s^{-1}\,Mpc^{-1}}$, $\Omega_\Lambda = 0.73$, $\Omega_\mathrm{M} = 0.27$ and a Chabrier initial mass function (IMF).

2 SAMPLE SELECTION

To investigate any redshift evolution of the AGN (s)SFR distribution, we use two samples of X-ray-selected AGNs: a low-z sample spanning $0.5 \leq z < 1.5$ and a high-z sample spanning $1.5 \leq z < 4$ (although the high-z sample is dominated by AGNs at $1.5 \leq z < 2.7$). The split at $z = 1.5$ is motivated by our ALMA target selection criteria: for this, we only consider AGNs with redshifts $>$1.5 since (a) the majority of $z < 1.5$ AGNs are detected with *Herschel* in the deepest fields and thus already have obscuration-independent SFR measures and (b) the negative k-correction at sub-mm wavelengths would call for prohibitive ALMA integration times.

The high-z sample were all selected from the 4 Ms *Chandra* Deep Field South (hereafter CDF-S) survey catalogue described in Xue et al. (2011) with updated redshifts from Hsu et al. (2014); we recalculate the rest-frame 2–10 keV luminosities (L_X) of the sources using these new redshifts. To ensure reliable AGN selection, we only consider those sources with $L_\mathrm{X} > 10^{42}$ erg s^{-1} and reliable redshifts (spec-z, or phot-z with $\Delta z/(1+z) < 0.1$) that lie within 6 arcmin of the average aim point of the survey (the latter ensures reliable positions for matching to ALMA counterparts). Our primary science goal of constraining the SFR distributions of AGN host galaxies in the context of the MS requires knowledge of the host galaxy stellar masses (M_*), which we derive following Santini et al. (2012). We refer to that study for a description of the relative uncertainties on M_*, which is estimated to be 50 and 20 per cent (1σ) for optically obscured (type 2) and unobscured (type 1) AGN, respectively. Since the majority (i.e. $>$70 per cent) of the AGNs in our samples are optically obscured, this level of uncertainty has no significant impact on our conclusions. We restrict our sample to AGNs with $M_* > 2 \times 10^{10}$ M$_\odot$; below this threshold, it becomes prohibitive to reach low enough flux limits to probe to SFRs significantly below the mean SFR of MS galaxies (hereafter SFR$_\mathrm{MS}$) with ALMA. Despite this M_* cut we still sample the vast majority of the luminous AGN population since the M_* distribution of $L_\mathrm{X} > 10^{42}$ erg s^{-1} AGNs peaks at $\approx 6 \times 10^{10}$ M$_\odot$ (e.g. Mullaney et al. 2012a).

The above selection returned 49 AGNs (our high-z sample), with 20 and 29 having spec-z and phot-z, respectively. Of these 49, 13 are detected in the GOODS–*Herschel* 160 μm maps of the CDF-S (Elbaz et al. 2011) from which SFRs are be derived. Of the remaining 36 AGNs, 24 were observed by ALMA. However, since making our original ALMA target list, a more sensitive *Herschel* 160 μm map of the CDF-S has been generated by combining the PEP (Lutz et al. 2011) and GOODS–*Herschel* surveys (Magnelli et al. 2013) and four of our 24 ALMA targets are now detected in that new map. For these four, we adopt the mean (s)SFR derived from the two facilities (see Section 3). All other *Herschel* fluxes and 3σ upper limits (including for the twelve *Herschel*-undetected AGNs not targeted by ALMA) are also taken from the combined PEP+GOODS–*Herschel* data set.

The low-z sample were selected from the regions of the *Chandra* Deep Field North (from Alexander et al. 2003 and adopting the same redshifts and M_* as Mullaney et al. 2012a) and South (Xue et al. 2011, but using the updated redshifts and M_*) surveys with *Herschel* coverage by the PEP+GOODS surveys. We also restrict this low-z sample to $L_\mathrm{X} > 10^{42}$ erg s^{-1} and $M_* > 2 \times 10^{10}$ M$_\odot$ to allow meaningful comparison with the high-z sample. This returned a sample of 110 AGNs (i.e. our low-z sample), 94 of which have spec-z. 65 of these 110 are detected in the *Herschel* 160 μm band, from which we derive (s)SFRs (see Section 3); 3σ flux upper limits were measured for the 45 *Herschel* non-detections.

3 ALMA OBSERVATIONS AND DATA ANALYSIS

All 24 of our ALMA targets were observed with ALMA Band-7 (i.e. observed-frame $\sim$850 μm) during 2013 November, with a longest baseline of 1.3 km. To maximize observing efficiency, the ALMA-targeted sample was split into three groups according to the flux limit required to probe down to at least SFR$_\mathrm{MS}$ at a given redshift. This corresponds to rms flux limits of 200, 125 and 90 μJy for the three groups. ALMA continuum fluxes were measured using `uv_fit` of GILDAS v.apr14c, adopting point source profiles for two unresolved sources and circular Gaussian profiles for the other five detected targets.

Measured ALMA and *Herschel* fluxes and upper limits were converted to 8–1000 μm infrared luminosities (hereafter L_IR) using our adopted redshifts (see Section 2) and the average infrared SEDs of MS galaxies described in Béthermin et al. (2015), which are constructed using the theoretical templates of Draine & Li (2007). However, we note that our conclusions do not change if we instead use either the Chary & Elbaz (2001) SEDs or a starburst SED (i.e. Arp220). At the redshifts of our high-z sample, Band-7 probes the rest-frame 180–340 μm, close to the peak of the far-infrared emission due to star formation. While these rest-frame wavelengths are also sensitive to dust mass (e.g. Scoville et al. 2014), based on the range of Draine & Li (2007) SED templates we estimate that the corresponding L_IR are accurate to within $\pm$0.3 dex, which we factor into our analyses. In a follow-up study we will employ full infrared SED fitting incorporating all available *Herschel* and ALMA fluxes and upper limits to reduce the uncertainties associated with the adopted SED, but such detailed fitting is beyond the scope of this Letter. As a check, however, we note that the SFRs derived from ALMA and *Herschel* data for the four AGNs that are detected with both are consistent to within this tolerance. SFRs are derived from L_IR using equation 4 from Kennicutt (1998), but adopting a Chabrier IMF. Finally, to explore the distributions of AGN host SFRs relative to SFR$_\mathrm{MS}$, we define $R_\mathrm{MS} \equiv \mathrm{SFR/SFR_{MS}}$, the relative offset from the MS, where SFR$_\mathrm{MS}$ is computed using equation 9 of Schreiber et al. (2015, hereafter S15).

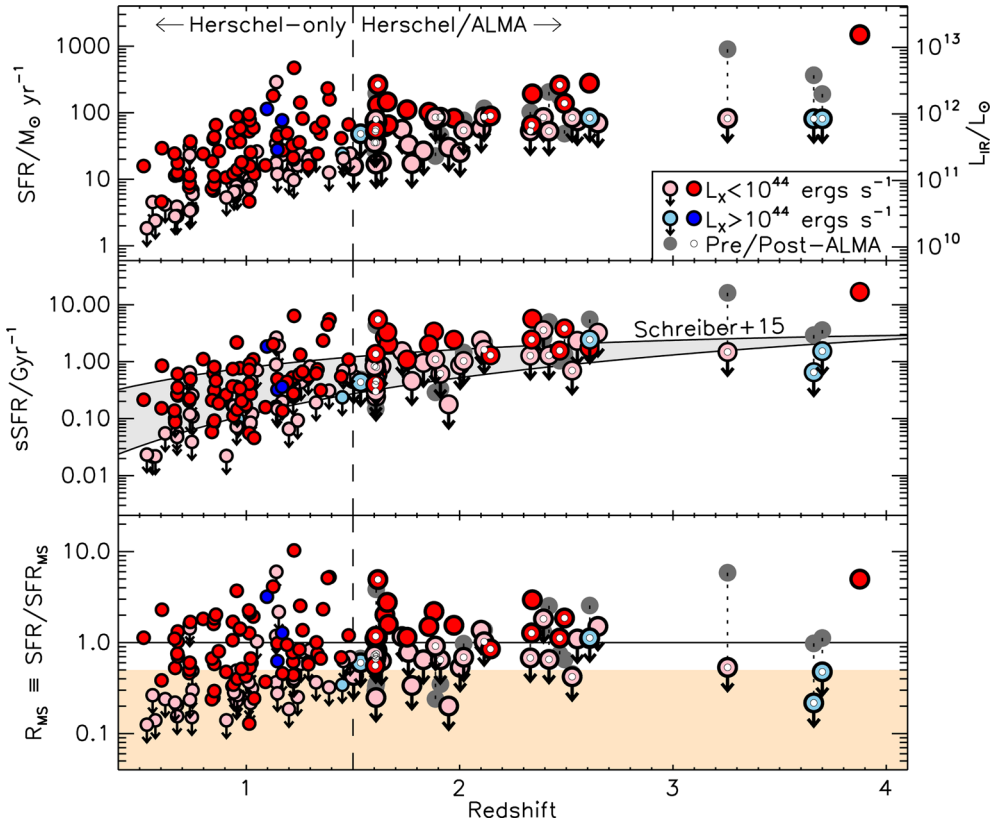

Figure 1. Host galaxy star-forming properties of our low-z (i.e. $0.5 < z < 1.5$; not observed by ALMA) and high-z (i.e. $z > 1.5$) samples of AGNs (samples separated by the vertical dashed line). In all plots, grey circles indicate pre-ALMA (specific) star formation rates ([s]SFRs) from *Herschel* which are connected to their ALMA-measured (s)SFRs by dotted lines. (s)SFRs from ALMA are indicated by small white circles. Red and blue circles represent AGNs with $L_X = 10^{42–44}$ erg s^{-1} and $L_X > 10^{44}$ erg s^{-1}, respectively, with lighter colours used for 3σ upper limits. Top: SFR versus redshift. Despite our ALMA observations probing SFRs up to a factor of ≈10 lower than *Herschel*, only ≈29 per cent of our ALMA-targeted AGNs are detected. Middle: sSFR versus redshift. In this panel, the shaded region represents the average sSFR of main-sequence (MS) galaxies (SFR_{MS}) as described by equation 9 of S15 for the stellar mass range of our sample. Bottom: R_{MS} versus redshift. By definition, the horizontal line represents the average R_{MS} of MS galaxies. Shading indicates where $R_{MS} < 0.5$. Between 34 and 55 per cent (dependent on upper limits) of AGNs in our combined (i.e. low-z+high-z) sample lie within this shaded region, compared to ≈15 per cent of MS galaxies.

4 RESULTS

4.1 Star-forming properties of X-ray AGNs

Despite our ALMA observations probing to SFRs up to a factor of ≈10 below that achieved with *Herschel* (Fig. 1, top) only seven (i.e. ≈29 per cent) of the 24 ALMA-targeted AGNs in our high-z sample are detected at $>3\sigma$ at 850 μm. The fractions of ALMA-undetected AGN are roughly the same for targets with spec-z and phot-z, suggesting that redshift uncertainties are not the primary cause of the non-detections. Despite the high fraction of non-detections, the 3σ upper limits provided by the ALMA+*Herschel* data enable us to infer the level of consistency between the distributions of R_{MS} for AGN and MS galaxies (see Section 4.2), with the latter having been shown not to vary in the M_* and redshifts ranges considered here (e.g. Rodighiero et al. 2011; Sargent et al. 2012).

To explore our AGN hosts' star-forming properties in the context of the evolving MS, we plot their sSFRs and R_{MS} values as a function of redshift (Fig. 1, middle and lower panels, respectively). We find that 54 to 88 (range due to upper limits) of the 159 AGNs (i.e. ≈34 to ≈55 per cent) in our combined (i.e. low-z + high-z) sample have $R_{MS} < 0.5$, with significant overlap between the fractions in our low-z (i.e. ≈43t to ≈54 per cent) and high-z (i.e. ≈14 to ≈59 per cent) samples. Comparing these fractions to the ≈15 per cent of MS galaxies with $R_{MS} < 0.5$ (from S15), reveals that the AGNs in our low-z sample, and possibly also our high-z sample, do not trace the same R_{MS} distribution as MS galaxies, instead displaying a strong bias towards lower R_{MS} values. Finally, we note that only ≈5 per cent of AGNs in our combined sample reside in starbursts (i.e. with $R_{MS} > 4$).

4.2 Parameterizing an X-ray AGN SFR distribution

With the large fraction of AGNs with $R_{MS} < 0.5$ in our combined and, in particular, low-z samples being inconsistent with the R_{MS} distribution of MS galaxies, we now attempt to place constraints on the distribution of SFRs (relative to the MS, i.e. R_{MS}) of AGN hosts. We place particular emphasis on quantifying the level of consistency/discrepancy between the AGN and MS R_{MS} distributions.

Our relatively small sample sizes, combined with the large fraction of non-detections prevent us from determining the AGN R_{MS} distribution directly. Since a key goal here is to quantitatively compare the AGN and MS R_{MS} distributions, we instead *assume* the same lognormal form for the AGN R_{MS} distribution as found for MS galaxies (e.g. Rodighiero et al. 2011; Sargent et al. 2012; S15):

$$N(R_{MS}) \propto \exp\left(-\frac{(\log(R_{MS}) - \mu)^2}{2\sigma^2}\right) \quad (1)$$

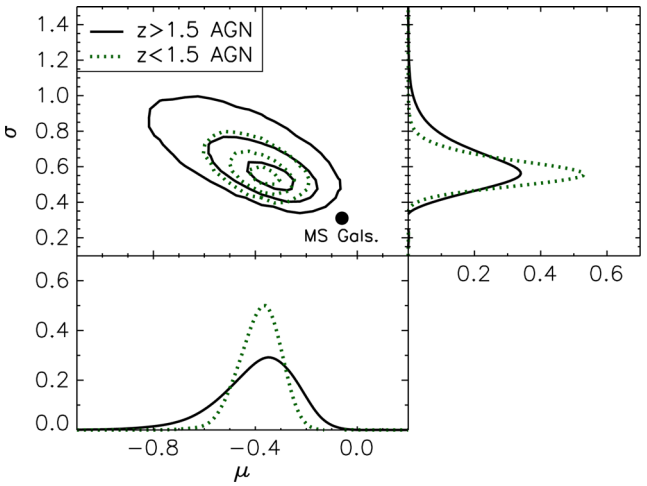

Figure 2. The posterior probability distributions (PDs) for the parameters describing the assumed lognormal $R_{\rm MS}$ distribution for AGN host galaxies: μ is the mode of the lognormal, while σ is its 1σ width (see equation 1). PDs for both our low-z and high-z samples are shown (see key). Contours of 20, 68 and 95 per cent confidence are shown. The best-fitting parameters of the combined (i.e. redshift-averaged) $R_{\rm MS}$ distribution of MS galaxies is indicated by the filled black circle (from Schreiber et al. 2015). The bottom and rightmost plots indicate the relative probability of μ and σ values; the location of the peak represent the most probable parameter values. When modelled as a lognormal, the $R_{\rm MS}$ distribution of AGN host galaxies is significantly broader, and shifted significantly lower than that of MS galaxies.

and infer its parameters (i.e. similar to Shao et al. 2010 who inferred the AGN $L_{\rm IR}$ distribution). This is done purely to ease comparison between the AGN and MS $R_{\rm MS}$ distributions by allowing us to compare like-for-like parameters (i.e. the mode, μ, and the variance, σ^2, of the lognormal $R_{\rm MS}$ distribution), and is not to be taken as a literal description of the true AGN $R_{\rm MS}$ distribution.[1]

We adopt a hierarchical Bayesian framework to determine the best-fitting parameters (i.e. μ and σ) for our assumed lognormal distributions, using Gibbs sampling and the Metropolis–Hastings MCMC algorithm to randomly sample their posterior probability distributions (hereafter, PDs; Gelman et al. 2014). The benefits of taking this approach are that (a) upper limits and uncertainties on $R_{\rm MS}$ can be readily taken into account and (b) the resulting posterior PDs provide us with meaningful parameter uncertainties. We use weak prior PDs, noting that the centring of these priors (within reasonable limits) has no significant effect on our results.

The posterior PDs on μ and σ for our two samples are presented in Fig. 2, while the best-fitting parameters (median of the PDs and 68 per cent confidence intervals) are given in Table 1. For comparison, we also include the best-fitting parameters of the lognormal $R_{\rm MS}$ distribution for non-AGN MS galaxies from S15. As expected from the smaller size of our AGN sample and the high fractions of non-detections compared to the MS galaxy sample of S15, the uncertainties on the posterior parameter values for the assumed AGN lognormal $R_{\rm MS}$ distribution are considerably larger than those for MS galaxies. Despite this, our analysis shows that the $R_{\rm MS}$ distributions of our low-z and high-z AGNs are both significantly broader and peak at significantly lower values (both at >99.9 per cent confidence) than that of MS galaxies (a similar result was recently obtained for z < 0.1 AGN from the Swift-BAT survey, Shimizu et al. 2015). Interestingly, our analyses show that, as with MS galaxies, there appears to be little evolution in the AGN $R_{\rm MS}$ distribution, with the modes and variances of the lognormal distributions describing our low-z and high-z samples being consistent to within 1σ. In light of this, we infer the $R_{\rm MS}$ distribution of our combined sample, which we find is roughly twice as broad as, and peaks ≈0.4 dex below, that of MS galaxies (Table 1).

[1] Investigating whether other forms better describe the $R_{\rm MS}$ distribution of AGN hosts will be the focus of a later study incorporating a larger set of ALMA observations from Cycle 2 (PI: Alexander; awaiting completion).

Table 1. Best-fitting parameters for the lognormal $R_{\rm MS}$(=SFR/SFR$_{\rm MS}$) distributions (see equation 1) of the samples of galaxies described in the main text.

(1) Sample	(2) μ	(3) σ
MS galaxies (Schreiber et al. 2015)	-0.06^a	0.31 ± 0.02
Low-z AGN sample	$-0.378^{+0.068}_{-0.079}$	$0.568^{+0.082}_{-0.062}$
High-z AGN sample	$-0.38^{+0.12}_{-0.16}$	$0.59^{+0.15}_{-0.10}$
Combined AGN sample	$-0.369^{+0.065}_{-0.080}$	$0.560^{+0.087}_{-0.065}$

Notes. Values given are the median of the posterior probability distributions (PDs) and the 68 per cent confidence intervals. [a]This is slightly offset from exactly zero as $R_{\rm MS}$ is the SFR relative to the *linear mean* SFR of MS galaxies, whereas μ is the mode of the $R_{\rm MS}$ distribution.

5 INTERPRETATION

In the previous section we used our combined ALMA+*Herschel* data to demonstrate that, when modelled as a lognormal, the AGN $R_{\rm MS}$ distribution is significantly broader and peaks at significantly lower values than that of MS galaxies. This appears to be at odds with recent findings based on mean-stacked *Herschel* data that the average star-forming properties of AGN hosts is consistent with those of MS galaxies (e.g. Mullaney et al. 2012a; Santini et al. 2012; Rosario et al. 2013). Here, we place our results in the context of these studies to explore the root of these apparent discrepancies.

When comparing to results derived from mean-stacked *Herschel* data, it is important to note that mean-stacking provides a linear mean which will not correspond to the mode, μ, of a lognormal distribution. Instead, the linear mean will *always* be higher than the mode, with the discrepancy between the two increasing as function of both μ and σ. Therefore, while results from mean-stacking still hold when interpreted as the linear mean, depending on the underlying distribution this may not necessarily correspond to the mode.

We compare our results against those from stacking by calculating the linear mean of our lognormal distributions, taking a Monte Carlo approach to sample the μ and σ PDs. This gives linear-mean AGN $R_{\rm MS}$ values (i.e. $\langle R_{\rm MS}\rangle$) of $0.99^{+0.23}_{-0.16}$ and $1.09^{+0.47}_{-0.25}$ for our low-z and high-z samples, respectively (Fig. 3). These values are remarkably close to the linear mean $R_{\rm MS}$ of MS galaxies (i.e. $\langle R_{\rm MS}\rangle \approx 1$) and are broadly consistent with the linear means calculated by mean-stacking *Herschel* 160 μm maps at the positions of our AGN (i.e. $\langle R_{\rm MS}\rangle = 0.81 \pm 0.12$ and 0.86 ± 0.15, respectively). We conclude that these linear-means are, indeed, influenced by the high tail of the broad $R_{\rm MS}$ distribution and may not necessarily give a reliable indication of the modal SFR of AGN hosts.

Despite finding that the $R_{\rm MS}$ distribution of AGN hosts is shifted towards lower values compared to MS galaxies, our results remain consistent with AGNs preferentially residing in galaxies with

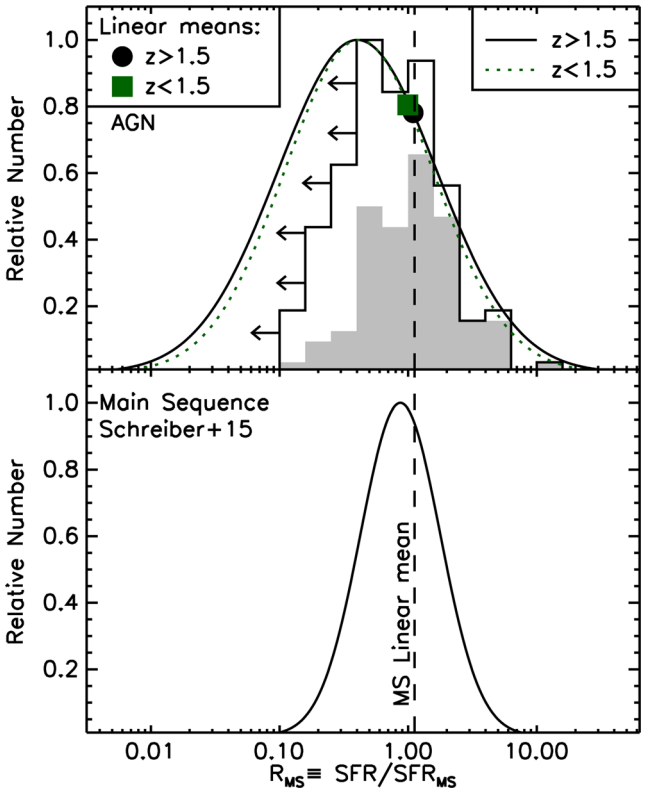

Figure 3. $R_{\rm MS}$ distributions for our high-z and low-z samples of X-ray-selected AGNs (top) and MS galaxies (bottom; from S15). Here, we show the lognormal distributions with best-fitting parameters shown in Table 1 (solid and dotted curves; see key). The histograms in the top panel shows the relative numbers of AGNs from our combined (i.e. low-z+high-z) sample in each $R_{\rm MS}$ bin; the solid grey histogram represents those AGNs detected at $>3\sigma$ with either *Herschel* or ALMA, whereas the empty histogram (with left-pointing arrows) also includes upper limits. The solid points in the top panel indicate the linear means of the lognormal distributions (equivalent to what would be obtained via, e.g. stacking analyses) and lie within 1σ of the linear mean $R_{\rm MS}$ of MS galaxies (vertical dashed line).

comparatively high (s)SFRs by $z \sim 0$ standards due to the strong redshift evolution of $\rm SFR_{MS}$. Indeed, applying our analyses to sSFR (rather than $R_{\rm MS}$) gives distributions peaking at $\approx$0.2 and $\approx$0.5 $\rm Gyr^{-1}$ for our low-z and high-z samples, respectively. To put this in context, $\langle \rm sSFR_{MS} \rangle \approx 0.1\,Gyr^{-1}$ at $z \approx 0$, thus local galaxies with sSFRs of 0.2 and 0.5 $\rm Gyr^{-1}$ would be classed as MS and starbursting galaxies, respectively.

Our result compare favourably to those derived from AGN surveys conducted at other wavelengths. For example, using SFRs derived from optical SED fitting, Bongiorno et al. (2012) reported a broad sSFR distribution for X-ray-selected AGNs that peaks below that of the MS at redshifts similar to those explored here (i.e. $0.3 < z < 2.5$). Similarly, Azadi et al. (2015) showed that the $R_{\rm MS}$ distribution of X-ray-selected AGNs (with a similar M_* selection as here) peaks at $\sim$0.1 and is similar to the $R_{\rm MS}$ distribution of M_*-matched galaxies (i.e. not just star-forming galaxies). As such, these studies and the results presented here support the view that X-ray-selected AGN hosts at moderate-to-high redshifts span the full range of *relative* sSFRs of $M_* \gtrsim 2 \times 10^{10}\,\rm M_\odot$ galaxies (e.g. Brusa et al. 2009; Georgakakis et al. 2014). However, with recent results suggesting that X-ray absorbed AGN may have higher SFRs than unabsorbed AGN (e.g. Juneau et al. 2013; Del Moro et al. 2015), it is feasible that alternative AGN selections may bring the AGN $R_{\rm MS}$ distribution closer to that of MS galaxies.

ACKNOWLEDGEMENTS

We thank the anonymous referee. DMA, ADM, CMH acknowledge STFC grant ST/I001573/1. This Letter makes use of ALMA data: ADS/JAO.ALMA#2012.1.00869.S.

REFERENCES

Alexander D. M., Hickox R. C., 2012, New Astron. Rev., 56, 93
Aird J., Coil A. L., Georgakakis A., Nandra K., Barro G., Prez-Gonzlez P. G., 2015, MNRAS, 451, 1892
Alexander D. M. et al., 2003, AJ, 126, 539
Azadi M. et al., 2015, ApJ, 806, 187
Béthermin M. et al., 2015, A&A, 573, A113
Bongiorno A. et al., 2012, MNRAS, 427, 3103
Brusa M. et al., 2009, A&A, 507, 1277
Chary R., Elbaz D., 2001, ApJ, 556, 562
Chen C.-T. J. et al., 2013, ApJ, 773, 3
Daddi E. et al., 2007, ApJ, 670, 156
Del Moro A. et al., 2015, preprint (arXiv:1504.03329)
Delvecchio I. et al., 2015, MNRAS, 449, 373
Draine B. T., Li A., 2007, ApJ, 657, 810
Elbaz D. et al., 2011, A&A, 533, A119
Gebhardt K. et al., 2000, ApJ, 539, L13
Gelman A., Carlin J. B., Stern H. S., Dunson D. B., Vehtari A., Rubin D. B., 2014, Bayesian Data Analysis, 3rd edn. CRC Press, Boca Raton, FL
Georgakakis A. et al., 2014, MNRAS, 440, 339
Harrison C. M. et al., 2012, ApJ, 760, L15
Hsu L.-T. et al., 2014, ApJ, 796, 60
Juneau S. et al., 2013, ApJ, 764, 176
Kennicutt R. C., Jr, 1998, ARA&A, 36, 189
Lutz D. et al., 2011, A&A, 532, A90
Magnelli B. et al., 2013, A&A, 553, A132
Mullaney J. R. et al., 2012a, MNRAS, 419, 95
Mullaney J. R. et al., 2012b, ApJ, 753, L30
Noeske K. G. et al., 2007, ApJ, 660, L43
Rodighiero G. et al., 2011, ApJ, 739, L40
Rodighiero G. et al., 2015, ApJ, 800, L10
Rosario D. J. et al., 2013, A&A, 560, A72
Rosario D. J. et al., 2015, A&A, 573, A85
Santini P. et al., 2012, A&A, 540, A109
Sargent M. T., Béthermin M., Daddi E., Elbaz D., 2012, ApJ, 747, L31
Schaye J. et al., 2015, MNRAS, 446, 521
Schreiber C. et al., 2015, A&A, 575, A74 (S15)
Scoville N. et al., 2014, ApJ, 783, 84
Shao L. et al., 2010, A&A, 518, L26
Shimizu T. T., Mushotzky R. F., Meléndez M., Koss M., Rosario D. J., 2015, MNRAS, 452, 1841
Silverman J. D. et al., 2008, ApJ, 679, 118
Stanley F. et al., 2015, preprint (arXiv:1502.07756)
Xue Y. Q. et al., 2011, ApJS, 195, 10

This paper has been typeset from a TEX/LATEX file prepared by the author.